Tropical Oceanography
ISSN 1679-3013 (online) / ISSN 1679-3005 (print)

INVESTIGATING OF THE TWO-CORE STRUCTURE OF THE ATLANTIC NORTH EQUATORIAL COUNTERCURRENT WITH THE GLORYS12V1 REANALYSIS

Djoirka M. DIMOUNE[1]*; Fabrice HERNANDEZ[1,2]; Moacyr ARAÚJO[1,3]

[1]Laboratório de Oceanografia Física Estuarina e Costeira (LOFEC), Departamento de Oceanografia da Universidade Federal de Pernambuco (UFPE), Cidade Universitária, Avenida Arquitetura s/n, 50740-550 Recife, PE, Brasil. E-mail: pmintodimoune@gmail.com
*Corresponding author

[2]LEGOS, Université de Toulouse, CNES, CNRS, IRD, UPS (Toulouse), 18 avenue Edouard Belin, 31400 France. E-mail: fabrice.hernandez@ird.fr

[3]Brazilian Research Network on Global Climate Change (Rede CLIMA), Av. dos Astronautas, 1758, 01227-010 São José dos Campos, SP, Brazil. E-mail: moa.ufpe@gmail.com

RESUMO. Vinte e seis anos de reanálise GLORYS12V1 foram utilizados para investigar a variabilidade da estrutura com dois núcleos da Contracorrente Norte Equatorial (CCNE) no Atlântico tropical. Os dois núcleos da NECC exibem posições médias de 6,3°N±1,4°/5,4°N±1,1° e 9,7°N±1°/8,9°N±0,9° na área oeste de 32°W/entre 22°-32°W. Ambas as áreas mostram um ciclo semianual da posição do núcleo sul com posições mais setentrionais em maio/março e julho/julho. O transporte do ramo associado ao núcleo sul mostra ciclos anuais com máximos em agosto (>17 Sv) e julho (7 Sv) que são influenciados respectivamente apenas pela força do rotacional do vento (FRV), mas também pela recirculação para leste do ramo norte da Corrente Sul Equatorial na bacia central. Ao contrário, o transporte do ramo norte da CCNE mostra os mesmos ciclos anuais, com máximos ocorrendo em setembro em ambas as áreas. A força da FRV liderou o transporte total da CCNE com 1 mês. 83%/71% deste transporte dentro dos primeiros 150 m de profundidade ocorre acima da termoclina na área oeste/central. No oeste, o transporte do ramo norte mostra variações anuais associadas à força da FRV enquanto a posição do núcleo sul na bacia central parece estar associada à migração da Zona de Convergência Intertropical.

Palavras-Chave: Atlântico tropical, Contracorrente Norte Equatorial, estrutura com dois núcleos, transporte de volume, rotacional do vento, reanálise GLORYS12V1

ABSTRACT. Twenty-six years of GLORYS12V1 reanalysis are used to investigate the variability of the two-core structure of the North Equatorial Countercurrent (NECC) in the tropical Atlantic. The NECC's two cores exhibit mean positions of 6.3°N±1.4°/5.4°N±1.1° and 9.7°N±1°/8.9°N±0.9° in the area west of 32°W/between 22°-32°W. Both areas witness a semi-annual cycle of the southern core position with northernmost positions in May/March and July/July. The transport of the branch associated to the southern core shows annual cycles with maxima in August (>17 Sv) and July (7 Sv) which are influenced respectively by only the wind stress curl (WSC) strength, but also by the eastward recirculation of the northern branch of the South Equatorial Current in the central basin. On the opposite, the NECC's northern branch transport shows the same annual cycles, with maxima occurring in September in both areas. The WSC strength led the NECC total transport by 1-month. 83%/71% of this transport within the first 150 m-depth occurs above the thermocline in the western/central area. In the West, the northern branch transport shows year-to-year variations associated with the WSC strength while the southern core position in the central basin appears to be associated with the Intertropical Convergence Zone migration.

Keywords: Tropical Atlantic, North Equatorial Countercurrent, Two-core structure, volume transport, wind stress curl, GLORYS12V1 reanalysis.

INTRODUCTION

In the tropical Atlantic (TA), one of the most important zonal surface currents is the North Equatorial Countercurrent (NECC), part of the complex TA wind-driven circulation. This current flows eastward between 3°-15°N across the basin, flanked by the North Equatorial Current (NEC) and the northern branch of the South Equatorial Current (nSEC) (Fig. 1). In the west, it is fed at the surface by the retroflected branch of the North Brazil Current Retroflection (rNBC) and transports fresher and oxygen-rich waters, and heat from the western boundary to the northern and the eastern basin (Philander and Pacanowski, 1986; Schott *et al.*, 2004; Urbano *et al.*, 2006; 2008; Castellanos *et al.*, 2015; Varona *et al.*, 2019). The North Equatorial Undercurrent (NEUC) also flows eastward underneath the NECC, fed by the subthermocline water from the rNBC, but is influenced by the waters from the nSEC, which are characterized by oxygen-poor waters (Burmeister *et al.*, 2019). The NECC and the NEUC are well separated in the western TA during the first half of the year when the NEUC is stronger, especially during the boreal spring, and are completely merged below the thermocline surface during the second half of the year (Urbano *et al.*, 2006).

To understand the seasonal variability of the TA circulation, many studies have been conducted so far to infer the NECC evolutions and their relationship with the wind's pattern variability. Garzoli and Katz (1983) analyzed the shallow water vorticity equation using historical hydrographic data and identified two main areas with different behaviors. Between 22°-42°W, the authors found that the NECC flow is in the Sverdrup balance. West of 42°W, this balance fails due to the importance of the nonlinear advective and local winds friction terms in the vorticity equation. In the first region, they found a delay of 1 to 2 months between the thermocline displacement and the wind stress curl (WSC) over the basin, which was explained by the influence of the westward propagating Rossby waves on the thermocline. Using numerical modeling, Verdy and Jochum (2005) confirm the importance of the nonlinear terms of the meridional and zonal advection of the mean flow and the eddies, which breaks down the balance between the divergence of the Ekman pumping and the divergence of the geostrophic currents. They also found that this region is extended to 32°W (area 1: Gray square in Fig. 1). Fonseca *et al.* (2004) and Urbano *et al.* (2006) confirmed this finding and showed that the NECC transport is approximately in Sverdrup balance but lags the WSC strength by 1 to 2 months. In particular, Urbano *et al.* (2006) used Acoustic Doppler Profilers (ADCP) and modeling at 35°W to investigate the two-core structure of the NECC previously mentioned by Schott and Böning (1991) and Didden and Schott (1992). They explained the one month lag found between the NECC's total transport from the surface to below the below thermocline and the "Sverdrup balance" transport at 35°W by the traveling time of the first mode baroclinic Rossby waves from the African coast to 35°W. Their results also showed that their model underestimates the NECC transports above the thermocline, overestimating a 1 to 2-month time lag. East of 32°W (area 2: Gray square in Fig.

1), both Garzoli and Katz (1983) and Verdy and Jochum (2005) found that the nonlinear terms effects on the seasonal variability of the transport of the NECC are negligible.

The purpose of this study is to investigate the two-core structure of the Atlantic North Equatorial Countercurrent (NECC) and the associated transport of both cores above the thermocline in relation to the seasonal variability of the remote wind blowing in the eastern basin as considered by Fonseca *et al.* (2004), represented by the blue rectangle in Fig. 1. However, they could not evidence any particular relationship at the interannual timescales due to the short 8-year available data period. Therefore, we propose to benefit from the longer time series (i.e., 1993-2018) provided by the state-of-art GLORYS12V1 global ocean reanalysis (G12V1) over the TA. This reanalysis has been proved to be globally realistic, particularly in the South Atlantic Ocean (e.g., Artana *et al.*, 2018, 2019; Poli *et al.*, 2020). To achieve our goal, areas 1 and 2 will be considered to investigate the influence of the wind fields on the NECC characteristics (branches and cores positions and associated transports).

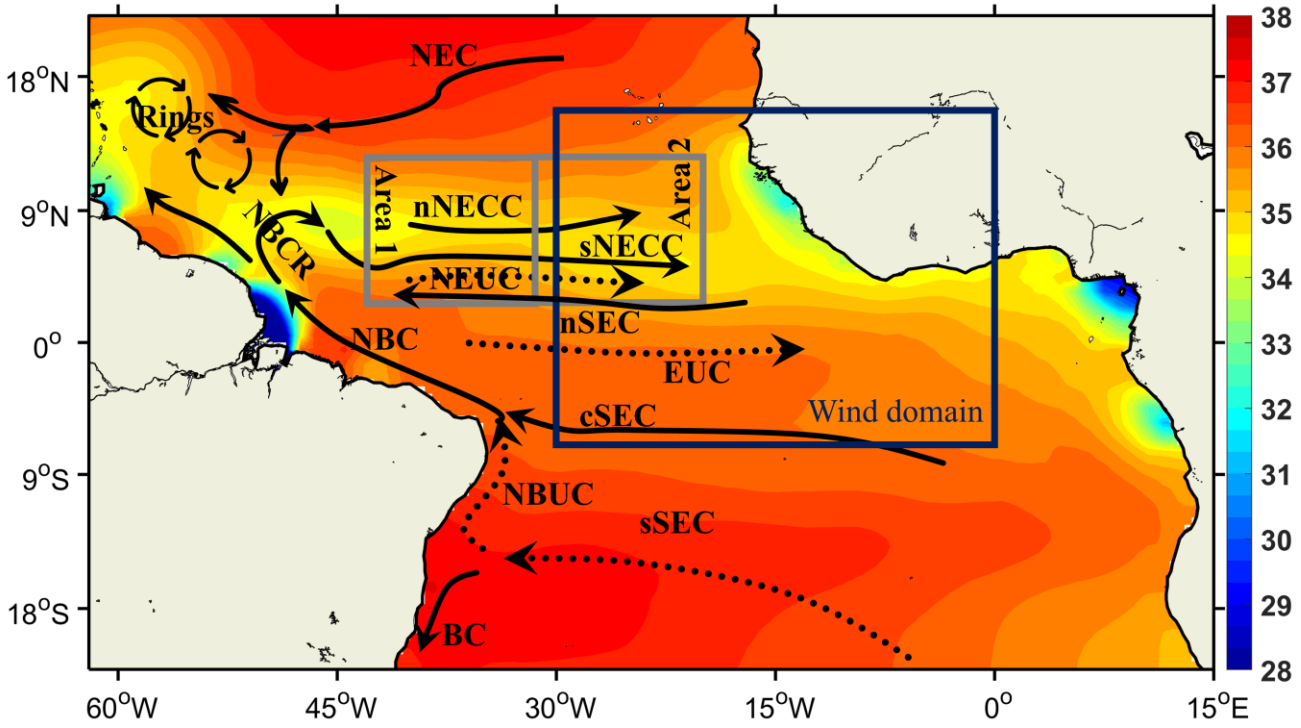

Figure 1. Mean Sea Surface Salinity (SSS) map for Sep-Oct-Nov averaged from 1993 to 2018 in the tropical Atlantic. Superimposed surface and thermocline currents (respectively thick solid and dashed black lines) in the study area based on John *et al.* (1990), Schott *et al.* (2004) and Halm *et al.* (2017): North Equatorial Current (NEC), North Equatorial Undercurrent (NEUC), North Equatorial Countercurrent (NECC), its northern branch (nNECC), Equatorial Undercurrent (EUC), southern, northern and central branches of the South Equatorial Current (sSEC, nSEC, cSEC), North Brazil Undercurrent (NBUC) North Brazil Current and its retroflection (respectively, NBC and NBCR) and the rings shed during the NBCR. The gray boxes define the region where the NECC parameters are calculated (area 1 and area 2); and the blue box define where the wind parameters are calculated. The SSS dataset used here is the CORA SSS reanalysis

(INSITU_GLO_TS_OA_REP_OBSERVATIONS_013_002_b product) made available by Copernicus Marine Service (CMEMS) at https://resources.marine.copernicus.eu/products.

1. DATA AND METHODS

Three datasets are used in this study:

1) The G12V1 reanalysis of monthly zonal current components (product name GLOBAL_REANALYSIS_PHY-001-030) available at the Copernicus Marine Service (CMEMS: https://marine.copernicus.eu/), with a 1/12° horizontal grid resolution and 50 irregular vertical levels from the surface to the bottom ocean. This reanalysis, comprehensively detailed and validated at global scale by Lellouche *et al.* (2018; 2021) is based on a 1/12° high resolution global ocean configuration using the NEMO model forced by the ECMWF ERA-Interim wind reanalysis. Its realism is obtained through data assimilation of along-track altimeter sea level anomaly (SLA), satellite sea surface temperature (SST), satellite sea ice concentration, and in situ temperature and salinity (T/S) vertical profiles from the CORA database corrected from the slowly evolving large-scale biases in temperature and salinity (Madec, 2008; Cabanes *et al.*, 2013; Good *et al.*, 2013; Lellouche *et al.*, 2018; 2021). Here, the zonal velocities have been extracted first in areas 1 (between 2°N– 15°N and 32°–42°W) and 2 (between 2°N– 15°N and 22°–32°W) over the 1993-2018 period. Then, they have been interpolated vertically with 1 m resolution, and finally, zonally averaged in each area.

2) The vertical profiles of G12V1 monthly temperature estimates have also been extracted and interpolated vertically with 1 m resolution, then zonally averaged in both areas. This allows computing the depth of the 21.5°C isotherm, usually considered the thermocline upper limit in the TA (e.g., Urbano *et al.*, 2006).

3) The monthly surface wind velocity fields from ERA5 provided by the European Centre for Medium-Range Weather Forecasts (ECMWF, http://www.ecmwf.int) in 1/4° grid have also been used to investigate the influence of the wind on the NECC over the same period. Following Fonseca *et al.* (2004), the wind stress components are zonally averaged in a region bounded by 6°S–16°N and 0°–30°W (Fig. 1) and are used to calculate the WSC. Its strength is obtained by the difference between its maximum negative and positive values every month. The WSC is also used to find the location of the ITCZ, determined by the position of the WSC zero value, following Fonseca *et al.* (2004).

2. CHARACTERIZATION OF THE TWO-CORE STRUCTURE OF THE NECC IN THE TROPICAL ATLANTIC

To show the two-core structure of the NECC, we compute the zonal current monthly climatology of the NECC in area 1 (Fig. 2) and area 2 (Fig. 3), considering the 1993-2018 period.

We distinguish near the surface over the year, one or two eastward branches of the NECC characterized by a vertical two-core structure, separated or not in both areas. The presence of the two-core structure in area 1 is consistent with Urbano *et al.* (2006). These NECC structures appear weaker in area 2, indicating that it weakens along their pathway. In area 1, the northern core of the NECC (nNECC) is permanent during the second half of the year, mostly from September to February; It appears fully separated from the southern core at the end of its cycle from December to February. For the rest of the year, the nNECC is only present some years. On the opposite, the sNECC is almost present all the year but is well established from October to December and from March to May when the nNECC is separated from the sNECC. The maximum (minimum) core velocity of the sNECC occurs in area 1 in October-November (May) with a value of 0.5 m/s (<0.1 m/s), while in the area 2, it occurs in June-July (March) with a value of 0.3 m/s (<0.05 m/s). In both areas, most of the NECC flows above the thermocline.

To characterize the two branches of the NECC associated with the two cores pattern, in order to calculate the transport associated with the branches (Fig. 4), particularly when the flow weakens in area 2, we calculate the depth-average of the zonal velocity from the surface to the mean depth of the thermocline in both areas. The mean depth climatology (Fig. 5c) exhibits averaged values over the year of 91 m ± 5 in area 1, and 68 m ± 4 in area 2. The values in both areas are consistent with those found by Garzoli and Katz (1983). This method aims to identify in each depth-averaged horizontal profile of the current the limit between the sNECC and the nNECC branches which in practice is the position of the lowest local minimum between two highest positive local maxima. The position of the two highest positive local maxima represents, in this case, the core position of each core/branch. The NECC is considered a unique branch (sNECC) when the depth-average of the zonal velocity exhibits either only one positive local maximum or several positive local maxima and no local minima. The NECC presents two separated branches when the lowest local maximum is negative. This method helps to find the sNECC and the nNECC core positions and compute the transport of the branches associated with the cores of the NECC illustrated by Fig. 4 over the years. The zonal transports are calculated following Burmeister *et al.* (2019) as follows:

$$Tr = \int_{Di}^{Df} \int_{Zs}^{Z} U.d\,x.dz \qquad / \mathbf{1} /$$

Where U is the eastward (positive velocity) flow; x is the latitude, converted into meters, and z is the depth of the water column, also in meters. Di and Df are respectively the lower and the higher latitude of U; and Zs and Z are respectively the reference depth at the surface, which is 0 m in this study, and the depth limit for calculating of the transport.

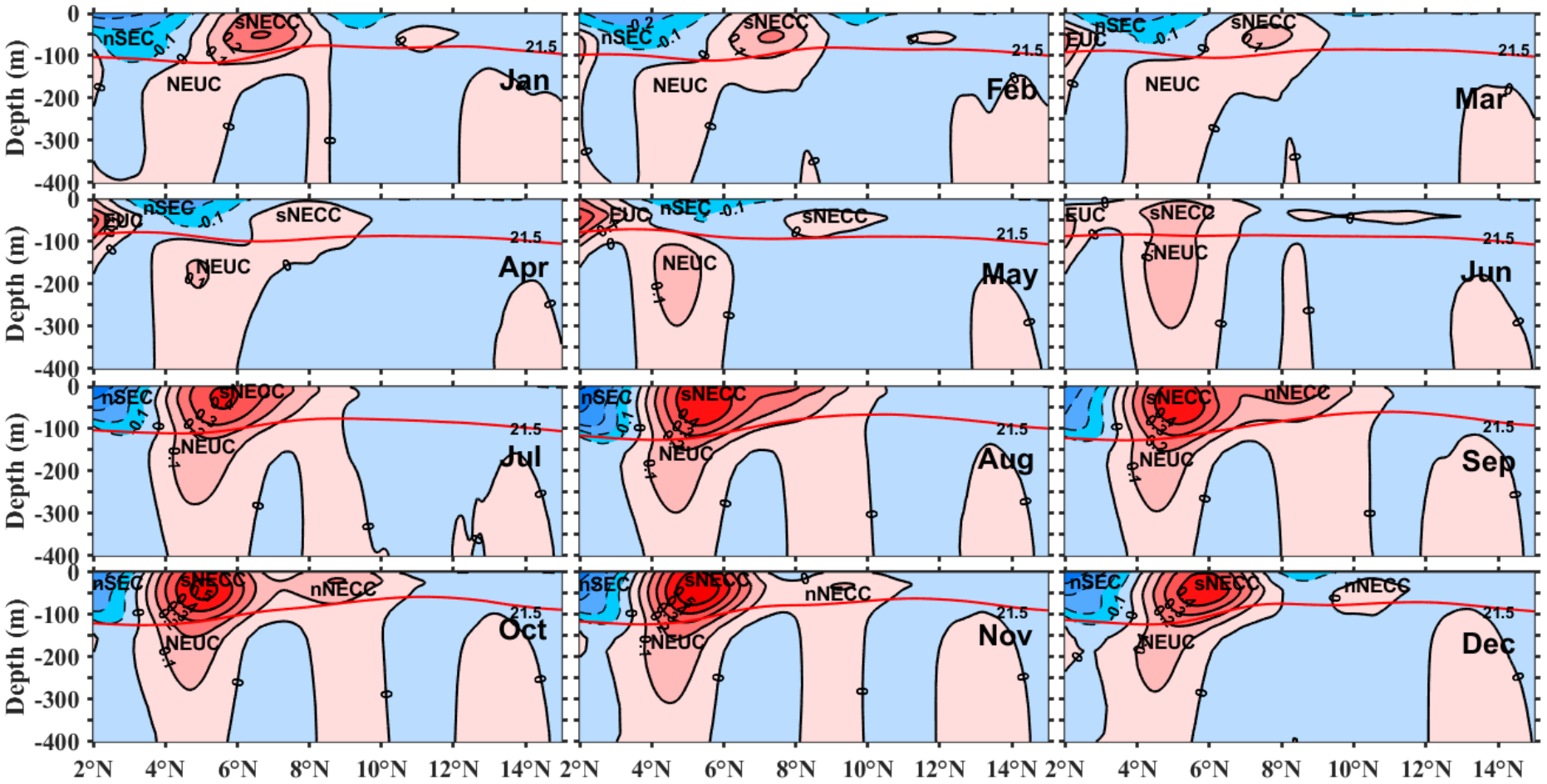

Figure 2. Monthly climatology of the meridional sections of G12V1 zonal velocity in area 1 (32°-42°W, 2°-15°N). The contour interval is 0.1 m/s, and dashed lines represent negative (westward) velocities also represented by the blue color. The red color represents the eastward velocities. The 21.5 °C isotherm is overlaid (red line) and represents TA thermocline upper limit.

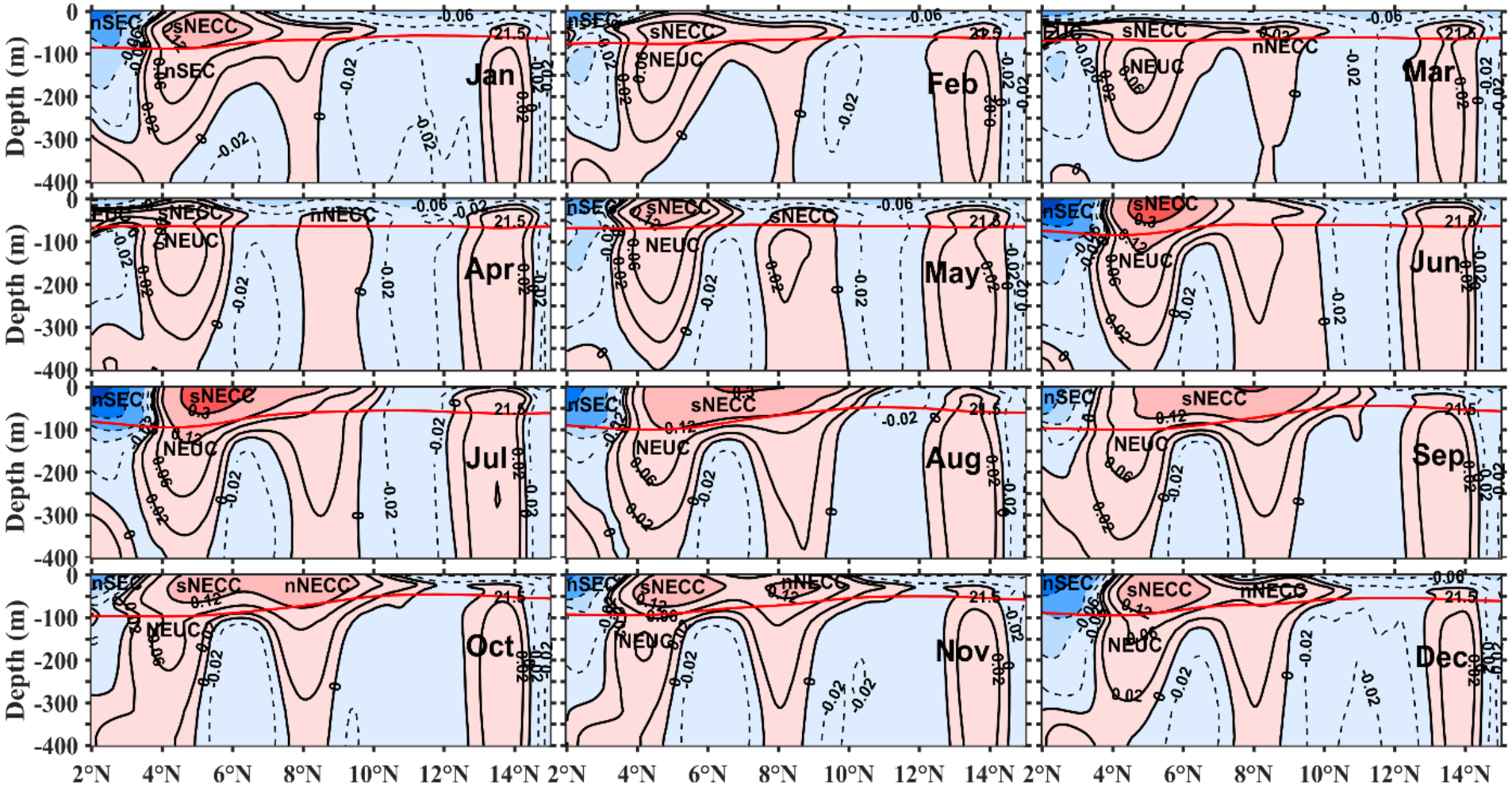

Figure 3. Monthly climatology of the meridional sections of G12V1 zonal velocity in area 1 (22°-32°W, 2°-15°N). The contour lines are irregular and represent isolines of the velocity of the currents. The dashed lines (blue color) represent negative (westward) velocities. The red colors show the eastward velocities. The 21.5 °C isotherm is overlaid (red line) and represents the TA thermocline upper limit.

3. VARIABILITY OF THE TWO CORES OF THE NECC AND THEIR ASSOCIATED TRANSPORTS IN AREAS 1 AND 2

The time series of the positions of the NECC cores and their associated transport above the thermocline (Fig. 4) show a strong seasonal variability, which is consistent with the variability of the tropical Atlantic (e.g., Garzoli and Katz, 1983; Garzoli and Richardson, 1989; Garzoli, 1992; Polonsky and Artamonov, 1997; Yang and Joyce, 2006). Fig. 4 also shows year-to-year variations. Our results show a larger NECC in area 1 than in area 2. Moreover, the mean location of the sNECC (nNECC) is at 6.3°N ± 1.4° (9.7°N ± 1°) in area 1, and 5.4°N ± 1.1° (8.9° ± 0.9°) in area 2. The sNECC (nNECC) core lies latitudinally between approximately 3.5°N (7.7°N) and 11.3°N (11.4°N) in area 1, and between 3.5°N (6.7°N) and 9.7°N (10.9°N) in area 2. Fonseca *et al.* (2004), who used 8 years of TOPEX/Poseidon altimeter-derived sea height anomaly and climatological hydrographic data, found the sNECC's core confined between 3°-10°N. Their methods for determining the NECC's location could not allow the identification of the northern core of the NECC, nor the core position of the weaker flow of the NECC between March and June. This might explain the difference in our results. The monthly climatology of NECC's core location (Fig. 5 b and e) also does not show the two northernmost locations of the sNECC in February and August for both areas. Our results show in area 1 a slightly northward migration of the sNECC from June to July, leading to a northern core of the NECC that starts growing and migrating northward from August to February in area 1. After February, the nNECC flow is weaker and shallower, and the core becomes difficult to capture by our method in area 1. In area 2, the mean location of the nNECC varies slightly. The root mean square (rms) of the mean monthly location in both areas shows larger values for the nNECC than the sNECC. This shows that the core position for the nNECC is more significant than for the sNECC, which is consistent with Urbano *et al.* (2006). The northward migration of the sNECC is clearly shown in both areas, respectively, between November and May in area 1, and November and March in area 2.

Table 1. Percentage of the transport of the NECC's branches above the thermocline relatively to the transport above 150 m-depth

Percentage of transport above thermocline in area 1			Percentage of transport above thermocline in area 2		
sNECC	nNECC	NECC	sNECC	nNECC	NECC
84%	70%	83%	74%	62%	71%

Before the analysis of the time series of transport of the NECC branches above the thermocline, the transports above 150 m-depth has also been calculated considering that the core of the NEUC is deeper than 150 m-depth (e.g., Urbano *et al.*, 2006) and its contribution to the NECC during the year is weaker above 150 m-depth. A comparison between the transports above the thermocline and above 150 m-depth (Tab. 1) shows higher percentages of transport above the thermocline in area 1 compared to area 2. The nNECC transport percentage above the

thermocline is lower, with 70% in area 1 and 62% in area 2. It indicates that a more significant part (>30%) of the nNECC remains between the thermocline surface and the 150 m-depth. The percentages of the sNECC transport and the total transport show values higher than 80% and 70% respectively in area 1 and area 2 and confirm that the sNECC is the main contributor to the total NECC transport in both areas. This also shows that the more significant part of the NECC transport is above the thermocline. The correlations between both transports (Figure not shown) for the branches and the total flow show significant correlations with a coefficient greater than 0.99 and 0.97, respectively, in area 1 and area 2. This shows that transports above 150-m can be used to study the NECC and investigate mechanisms which drive its seasonal and interannual variability.

The analysis of the time series of the transports of the NECC branches above the thermocline (Fig. 4a, i, d, and l) shows higher values as expected in area 1 compared to area 2. The transport of the sNECC (nNECC) varies from approximately 0 to 21 Sv (0 to 7.2 Sv) in area 1 compared to 0 to 11 Sv (0 to 8.3 Sv) in area 2. Maximum values of the sNECC transport in area 1, associated with locations of the core at about 5.4°N, usually occur during August, in good agreement with the Sverdrup transport proposed by Urbano *et al.* (2006). In area 2, we find an earlier maximum in July at about 5.3°N (Figs. 5a and 5d). Maximum values of the nNECC transport in both areas occur in September, associated with locations of the cores at about 8.5°N. Overall, the NECC is weaker during the first half of the year. Then stronger during July and August for the sNECC and September for the nNECC. The rms values during the first half of the year witnessed the weak variability of the NECC, which is very weak or even disappears during this period.

The relationship between the transport and the location of the NECC's cores shows two different scenarios for area 1 and area 2 (Figs. 4a, 4d, 5a, 5b, and 4i, 4l, 5d, 5e). In area 1, during the onset phase of the sNECC in June–July, the current witnesses an increase in its strength and location. The current shifts southward after while its strength continues to increase. The maximum strength of the sNECC occurs in August when the ITCZ reaches its northernmost position. The sNECC remains about the same location until November. Then it moves northward again when the nNECC is about 9.8°N. In area 2, the onset phase of the sNECC starts in April-May. Its branch witnesses an increase in strength and location until July, followed by a decrease of both strength and location until October-November when the nNECC migrates northward. The onset phase of the nNECC transports in areas 1 and 2 are similar and starts between July and August, two months later than the onset of the sNECC in area 1. The maximum strength of the nNECC occurs in September, one month later than the northernmost position of the ITCZ in August, and decreases after when the nNECC is still moving northward.

The monthly anomalies relative to the monthly climatology of the NECC's location and the transport-associated to the corresponding cores do not show any persistent patterns or obvious correlation for the sNECC over the period investigated. However, the location and transport show significant anomalies relative to their climatological values during specific years. For example, the monthly anomalies of the sNECC location were atypically far north (south) in 1995 and 2009 (1996, 1999, and 2012), and the monthly anomalies of the sNECC transport were unusually strong (weak) in 1994, 1996, and 2017 (1995 and 2009). The strong anomalies between 1993 and 2000 were also found by Fonseca *et al.* (2004). In area 2, the correlation between the core position of the sNECC and the associated transport is higher than in area 1 (0.34). Between area 1 and area 2, some coincident anomalies are found for the transport of the sNECC during the years 1994, 1995, and 1996. The highest correlations are found between the nNECC's location and its cores associated transports (-0.41 and -0.60 for areas 1 and 2). The correlation of area 2 shows that strong (weak) nNECC indicates a southernmost (northernmost) location of its core. We remind the correlations mentioned above are significant with 95% of confidence level, performing the Student test.

4. THE RELATIONSHIP BETWEEN THE NORTH EQUATORIAL COUNTERCURRENT AND THE WIND FIELDS IN AREA 1 AND AREA 2

To investigate the relationship between the NECC and the wind in TA, the wind domain, shown in Fig. 1, has been used to compute the minimum and maximum zonally averaged WSC. Then deduce the WSC strength as the difference between these maximum and minimum WSC values following Fonseca *et al.* (2004). The ITCZ has been identified as the location of the WSC zero value. As found by Fonseca *et al.* (2004), the annual cycle of the ITCZ varies between its northernmost location at 9°N in August and the southernmost location at 1°N in March. The WSC strength minimum is also found in March (Fig. 5f). Unlike Fonseca *et al.* (2004), who found the peak of the maximum negative WSC in July, we found a peak in August, coinciding with the maximum WSC strength and the northernmost position of the ITCZ (Fig. 5f). The difference with our result can be due to the short length of the time series considered for their studies or the errors in satellite data used.

In the TA, the NECC transport is related to the influence of both the positive WSC north of the ITCZ and the negative WSC south of the ITCZ, and by the way, their difference is represented by the WSC strength (Fonseca *et al.*, 2004). In area 1, the maximum total transport occurs in September (Fig. 5a), and the minimum total transport occurs in May. The one to two-month lags of the NECC transport relative to the WSC strength cycle is consistent with expected delays due to Rossby wave propagation in the area (e.g., Garzoli and Katz, 1983, Urbano *et al.*, 2006). The sNECC and nNECC transport peaks in August and September, respectively, show that the phase lag between the WSC strength and the thermocline occurs in the nNECC region.

In area 2, the total transport of the NECC follows exactly the cycle of the WSC strength with a minimum in March and maximum in August with no lag. However, the transport associated with the NECC branches shows different cycles with different maximum. The transport- associated to the sNECC grows from April and reaches its maximum in July, one month before the peak of the WSC strength. Rosell-Fieschi *et al.* (2015) show that from April to July-August, the NECC is fed by an eastward retroflected branch of the nSEC which reaches its maximum during June-July in the central Atlantic and follows the ITCZ displacement. Burmeister *et al.* (2019) also show that the NEUC is supplied by the nSEC during this period and strengthens when the thermocline is shoaling (Xie and Carton, 2004). This means that the transport of the sNECC in area 2 should be influenced by the nSEC and the NEUC. In Fig. 3, the uniform flow reaching the surface in April strengthens later, then migrates northward should be composed of a mixture of the nSEC eastward recirculating branch and the NEUC. The nNECC transport shows the same seasonal cycle for area 1, which confirms our findings that the phase lag between the WSC strength and the thermocline occurs in the region of its branching in the TA. The one-month lag delay in area 2 is consistent with Garzoli and Katz (1983) and Urbano *et al.* (2006) findings.

The July-August northernmost location of the sNECC in both areas (Figs. 5b and 5e) coincides with the northernmost location of the ITCZ. Fonseca *et al.* (2004) found the same results. This suggests that the location of the sNECC during March-August is wind-driven. This confirms previous findings of Richardson and McKee (1984), Richardson and Reverdin (1987), Garzoli and Richardson (1989). Furthermore, the northward migration of the sNECC is consistent with Urbano *et al.* (2008) that found during this period a presence of zero line of the WSC north of 10°N that should influence this migration. Therefore, we assume that the northward migration of the nNECC from August to February should be due to the same mechanism, primarily in area 1.

At interannual timescales, correlations between the WSC strength monthly anomalies of the ITCZ and the monthly anomalies of the location of the NECC cores and the associated transports are not significant. Thus, to investigate the influence of the maximum WSC strength and the NECC's northernmost position due to the ITCZ, we performed a 3-month running mean of the maximum values of the WSC and the highest positions of the ITCZ for each year. They were correlated with the 3-month running averages of the locations of the cores and their associated transport. Correlations were significant only for nNECC, which shows a 0.52 correlation between its associated transport and the WSC strength in area 1 during September; and -0.59 between its core location and the ITCZ in June. This means that, on interannual timescales, the variability of the nNECC's location and its associated core transport might be related to the variability of the wind fields. The result opens the door for future investigations to infer the possible mechanisms that drive the two-core structure of the NECC and their associated transport on interannual timescales.

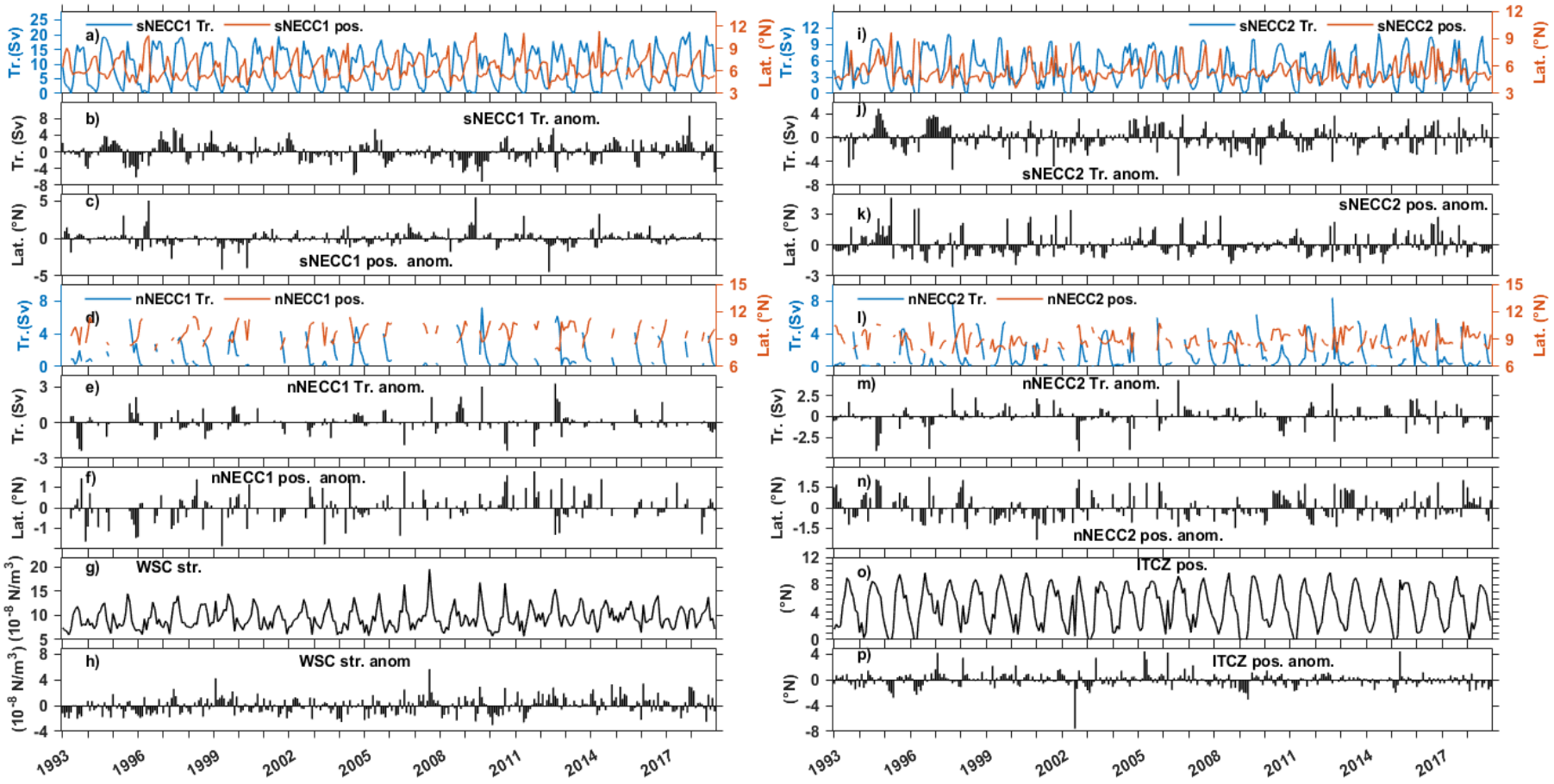

Figure 4. Time series of the core positions of the southern and northern branches of the North Equatorial Countercurrent (respectively, sNECC and nNECC), the transport above the thermocline associated to the cores and their anomalies in area 1 (first column: a-f) and in area 2 (second column: i-n), together with the time series of the wind stress curl (WSC) strength and the Intertropical Convergence Zone (ITCZ) position and their anomalies (respectively, g-h and o-p). (a and i) position of the sNECC core (orange line) and its associated transport (blue line) respectively, in area 1 and area2; (b and j) and (c and k) monthly anomalies of respectively, the position of the sNECC core and its associated transports in area 1 and area 2. (d and l) position of the nNECC core (orange line) and its associated transport (blue line) respectively,in area 1 and area2, (e and m) and (f and n) monthly anomalies of respectively,the position of the nNECC core and its associated transports in area 1 and area 2. (g and o) WSC strength and ITCZ position in the tropical Atlantic, respectively; and (h and p) their monthly anomalies.

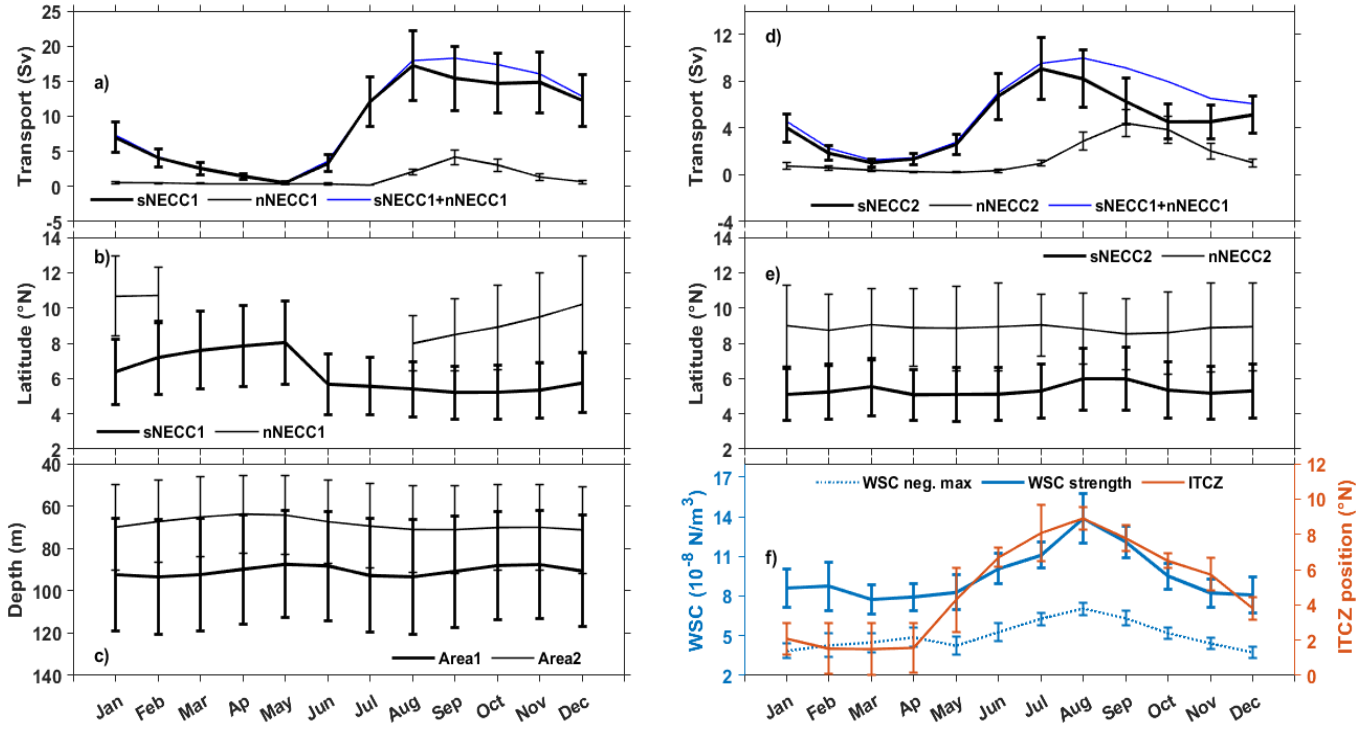

Figure 5. Monthly climatology from 1993 to 2018, of (a and d) the transport of the branches of the NECC, respectively in area 1 and area 2 (thick line: sNECC; thin line: nNECC and blue line: sum of both branches); (b and e) the position of the sNECC core (thick line) and the nNECC core (thin line), respectively in area 1 and area 2; (e) the mean depth of the thermocline in area 1 (thick line) and area 2 (thin line); and (f) the wind parameters: position of the ITCZ (orange line), WSC strength (thick blue line) and absolute value of the maximum in the negative WSC (thin blue line). The vertical bars indicate the root mean square values for each month.

CONCLUSION

This study using the GLORYS12V1 reanalysis, aims to re-visit the variability of the location of both cores of the NECC and their associated transport in relation to the wind fields blowing over the Tropical Atlantic. We found that G12V1 represents the NECC system consistent with previous studies of Garzoli and Katz (1983). In the past, Urbano *et al.* (2006) showed inconsistency between the NECC transport estimated from their model and a transport that would be solely due to ocean circulation response to the wind forcing using the Sverdrup balance. We found here that G12V1 NECC transport seasonal cycle does not present this inconsistency. It appears that this is caused by an underestimation of the NECC transport above the thermocline.

Our results also show the importance of considering the second core/branch of the NECC, the wind fields' influence on the entire NECC system at the seasonal timescales, and mainly on the nNECC on the interannual timescales. However, some investigations still need to be made, especially on interannual timescales. For example, Góes and Wainer (2003) used numerical modeling results to show that the long period wind variability was linked to warm and cold events

in the tropical Atlantic which impacted the strength of the tropical Atlantic circulation. Recently, Hormann *et al.* (2012) used altimetry data in the tropical Atlantic to show the influence of the Atlantic zonal mode on the NECC strength and the meridional mode on its location. Therefore, future studies might investigate the variability of the NECC two-core structures with the tropical Atlantic modes. In addition, specific vessel measured sections can also be used in the NECC regions to understand better the NECC's behavior at the seasonal and interannual timescales.

ACKNOWLEDGMENTS

We are grateful to the CMEMS and the ECMWF who made available the ocean reanalysis, and the mean wind fields for this work. We are also thankful to CAPES Foundation. Fabrice Hernandez supervised this work as part of the TAPIOCA Laboratoire Mixte International funded by IRD and CAPES/MEC in Brazil. Moacyr Araujo thanks the support of the Brazilian Research Network on Global Climate Change FINEP/Rede CLIMA (grants 01.13.0353-00). This work has been supported by the French LEFE/GMMC funded project Merca2Recife (42-DS-GMMC-MERCA2RECIFE – REF. CNRS N° 197932) and represents a contribution to the INCT AmbTropic, the Brazilian National Institute of Science and Technology for Tropical Marine Environments, CNPq/FAPESB (grants 565054/2010-4 and 8936/2011 and 465634/2014-1), and to the TRIATLAS project, which has received funding from the European Union's Horizon 2020 research and innovation program under grant agreement No 817578.

REFERENCES

Artana, C., Lellouche, J.-M., Sennéchael, N. and Provost, C. (2018), The Open-Ocean Side of the Malvinas Current in Argo Floats and 24 Years of Mercator Ocean High-Resolution (1/12) Physical Reanalysis, *Journal of Geophysical Research*: Oceans, Vol. 123, n. 11 , pp. 8489–8507, doi:10.1029/2018jc014528.

Artana, C., Provost, C., Lellouche, J. M., Rio, M. H., Ferrari, R., and Sennéchael, N. (2019). The Malvinas current at the confluence with the Brazil current: Inferences from 25 years of Mercator ocean reanalysis. *Journal of Geophysical Research: Oceans*, *124*(10), 7178-7200, doi:10.1029/2019jc015289.

Burmeister K., Lübbecke, J. F.,Brandt, P. and Duteil, O. (2019), Interannual variability of the Atlantic North Equatorial Undercurrent and its impact on oxygen, *Journal of Geophysical Research*: Oceans, Vol. 124, pp. 2348–2373, doi: 10.1029/2018JC014760.

Cabanes, C., Grouazel, A., von Schuckmann, K., Hamon, M., Turpin, V., Coatanoan, C. *et al.* (2013), The CORA dataset: validation and diagnostics of in-situ ocean temperature and salinity measurements, *Ocean Science*, Vol. 9, n. 1, pp. 1-18, doi: 10.5194/os-9-1-2013.

Castellanos, P., Pelegrí, J.L., Campos, E.J.D., Rosell-Fieschi, M. and Gasser, M. (2015), Response of the surface tropical Atlantic Ocean to wind forcing, *Progress in Oceanography*, pp. 134271-292, doi: 10.1016/j.pocean.2015.02.005.

Didden, N. and Schott, F. (1992), Seasonal variations in the western tropical Atlantic: Surface circulation from Geosat altimetry and WOCE model results, *Journal of Geophysical Research*: Oceans, Vol. 97, n. C3, pp. 3529-3541, doi: 10.1029/91jc02860.

Fonseca, C. A., Goni, G. J., Johns, W. E., and Campos, E. J. (2004). Investigation of the north Brazil current retroflection and north equatorial countercurrent variability. *Geophysical Research Letters*, *31*(21), doi:10.1029/2004gl020054.

Garzoli, S.L. and Katz, E.J. (1983), The Forced Annual Reversal of the Atlantic North Equatorial Countercurrent, *Journal of Physical Oceanography*, Vol. 13, n. 11, pp. 2082-2090, doi: 10.1175/1520-0485(1983)013<2082:Tfarot>2.0.Co;2.

Garzoli, S.L. and Richardson, P.L. (1989), Low-frequency meandering of the Atlantic North Equatorial Countercurrent, *Journal of Geophysical Research*: Oceans, Vol. 94, n. C2, pp. 2079-2090, doi: 10.1029/JC094iC02p02079.

Garzoli, S.L. (1992), The Atlantic North Equatorial Countercurrent: Models and observations, *Journal of Geophysical Research*: Oceans, Vol. 97, n. C11, pp. 17931-17946, doi: 10.1029/92jc01363.

Góes, M., and Wainer, I. (2003). Equatorial currents transport changes for extreme warm and cold events in the Atlantic Ocean. *Geophysical research letters*, Vol. 30, n.5, doi: 10.1029/2002GL015707.

Good, S.A., Martin, M.J. and Rayner, N.A. (2013), EN4: Quality controlled ocean temperature and salinity profiles and monthly objective analyses with uncertainty estimates, *Journal of Geophysical Research*: Oceans, Vol. 118, n. 12, pp. 6704-6716, doi: 10.1002/2013jc009067.

Hormann, V., Lumpkin, R., and Foltz, G. R. (2012). Interannual North Equatorial Countercurrent variability and its relation to tropical Atlantic climate modes. *Journal of Geophysical Research: Oceans*, Vol. 117, n. C4, doi: 10.1029/2011jc007697.

Lellouche, J.-M., Greiner, E., Le Galloudec, O., Garric, G., Regnier, C., Drevillon, M. *et al.* (2018), Recent updates to the Copernicus Marine Service Global ocean monitoring and forecasting real-time 1/12° high-resolution system, *Ocean Science*, Vol. 14, n. 5, pp. 1093-1126, doi: 10.5194/os-14-1093-2018.

Jean-Michel, L., Eric, G., Romain, B. B., Gilles, G., Angélique, M., Marie, D. *et al.* (2021). The Copernicus global 1/12° oceanic and sea ice GLORYS12 reanalysis. *Frontiers in Earth Science*, Vol. *9*, pp. 585, doi: 10.3389/feart.2021.698876.

Madec, G. (2008), *NEMO ocean engine - Version 3.1*, Note du Pôle de modélisation, (27), edited by Institut Pierre-Simon Laplace (IPSL), Paris, France, 201 p.

Philander, S.G.H. and Pacanowski, R.C. (1986), The mass and heat budget in a model of the tropical Atlantic Ocean, *Journal of Geophysical Research*: Oceans, Vol. 91, n. C12, pp. 14212-14220, doi: 10.1029/JC091iC12p14212.

Poli, L., Artana, C., Provost, C., Sirven, J., Sennéchael, N., Cuypers, Y. *et al.* (2020). Anatomy of subinertial waves along the Patagonian shelf break in a 1/12° global operational model. *Journal of Geophysical Research: Oceans*, *125*(12), doi:10.1029/2020jc016549.

Polonsky, A.B. and Artamonov, Y.V. (1997), North Equatorial Counter- current in the tropical Atlantic: Multi-jet structure and seasonal variability, *Ocean Dynamics*, Vol. 49, pp. 477–495, doi: 10.1007/bf02764342.

Richardson, P.L. and McKee, T.K. (1984), Average seasonal variation of the Atlantic equatorial currents from historical ship-drifts, *Journal of Physical Oceanography*, Vol. 14, pp. 1226–1238, doi: 10.1175/1520-0485(1984)014<1226:ASVOTA>2.0.CO;2.

Richardson, P.L. and Reverdin, G. (1987), Seasonal cycle of velocity in the Atlantic North Equatorial Countercurrent as measured by surface drifters, current meters, and ship drifts, *Journal of Geophysical Research*: Oceans, Vol. 92, n. C4, pp. 3691-3708, doi: 10.1029/JC092iC04p03691.

Rosell-Fieschi, M., Pelegrí, J.L. and Gourrion, J. (2015), Zonal jets in the equatorial Atlantic Ocean, *Progress in Oceanography,* Vol. 130, pp. 1–18, doi: 10.1007/bf02764342.

Schott, F.A. and Böning C.W. (1991), The WOCE model in the western equatorial Atlantic: Upper layer circulation, *Journal of Geophysical Research*: Oceans, Vol. 96, n. C4, pp. 6993-7004, doi: 10.1029/90jc02683.

Schott, F.A., McCreary, J.P. and Johnson, G.C. (2004), Shallow overturning circulations of the tropical–subtropical oceans, In: Wang, C., Carton, J. and Xie, S.-P. (Eds.), *Ocean–Atmosphere Interaction and Climate Variability,* AGU, Washington, pp. 261– 304.

Urbano, D.F., Jochum, M. and da Silveira, I.C.A. (2006), Rediscovering the second core of the Atlantic NECC, *Ocean Modelling*, Vol. 12, n. 1, pp. 1-15, doi: 10.1016/j.ocemod.2005.04.003.

Urbano, D. F., De Almeida, R. A. F., and Nobre, P. (2008). Equatorial Undercurrent and North Equatorial Countercurrent at 38 W: A new perspective from direct velocity data. *Journal of Geophysical Research: Oceans*, *113*(C4), doi: 10.1029/2007jc004215.

Varona, H.L., Veleda, D., Silva, M., Cintra, M. and Araujo, M. (2019), Amazon River plume influence on Western Tropical Atlantic dynamic variability, *Dynamics of Atmospheres and Oceans*, Vol. 85, pp. 1-15, doi: 10.1016/j.dynatmoce.2018.10.002.

Verdy, A. and Jochum, M. (2005), A note on the validity of the Sverdrup balance in the Atlantic North Equatorial Countercurrent, *Deep Sea Research Part I*: Oceanographic Research Papers, Vol. 52, n. 1, pp. 179-188, doi: 10.1016/j.dsr.2004.05.014.

Xie, S. and Carton, J. (2004), Tropical Atlantic variability: Patterns, mechanisms, and impacts, *Geophysical Monograph Series*, Vol. 147, pp. 121–142, doi: 10.1029/147GM07.

Yang, J. and Joyce, T.M. (2006), Local and equatorial forcing of seasonal variations of the North Equatorial Countercurrent in the Atlantic Ocean, *Journal of Physical Oceanography*, Vol. 36, pp. 238–254, doi: 10.1175/JPO2848.1.